Hindawi
International Journal of Antennas and Propagation
Volume 2019, Article ID 3924569, 11 pages
https://doi.org/10.1155/2019/3924569

Research Article

Two 2-D DOA Estimation Methods with Full and Partial Generalized Virtual Aperture Extension Technology

Riheng Wu[1], **Yangyang Dong**[2], **Zhenhai Zhang**[3] **and Le Xu**[4]

[1]*The Department of Information Engineering, Wenjing College, Yantai University, Yantai 264005, China*
[2]*The School of Electrical Engineering, Xidian University, Xi'an 710071, China*
[3]*The School of Mechatronics Engineering, The Beijing Institute of Technology, Beijing 100081, China*
[4]*The College of Electronic and Information Engineering, Nanjing University of Aeronautics and Astronautics, Nanjing 210000, China*

Correspondence should be addressed to Riheng Wu; riheng_w@163.com

Received 28 March 2019; Revised 28 April 2019; Accepted 10 December 2019; Published 24 December 2019

Academic Editor: Chien-Jen Wang

We address the two-dimensional direction-of-arrival (2-D DOA) estimation problem for L-shaped uniform linear array (ULA) using two kinds of approaches represented by the subspace-like method and the sparse reconstruction method. Particular interest emphasizes on exploiting the generalized conjugate symmetry property of L-shaped ULA to maximize the virtual array aperture for two kinds of approaches. The subspace-like method develops the rotational invariance property of the full virtual received data model by introducing two azimuths and two elevation selection matrices. As a consequence, the problem to estimate azimuths represented by an eigenvalue matrix can be first solved by applying the eigenvalue decomposition (EVD) to a known nonsingular matrix, and the angles pairing is automatically implemented via the associate eigenvector. For the sparse reconstruction method, first, we give a lemma to verify that the received data model is equivalent to its dictionary-based sparse representation under certain mild conditions, and the uniqueness of solutions is guaranteed by assuming azimuth and elevation indices to lie on different rows and columns of sparse signal cross-correlation matrix; we then derive two kinds of data models to reconstruct sparse 2-D DOA via M-FOCUSS with and without compressive sensing (CS) involvements; finally, the numerical simulations validate the proposed approaches outperform the existing methods at a low or moderate complexity cost.

1. Introduction

The 2-D DOA estimation has received considerable attention in the past decades and has met many applications in array signal processing society, such as, radar, sonar, and wireless communications [1]. Numerous array structures, such as L-shaped arrays, rectangular arrays, circular arrays, two parallel ULAs, etc., [2–9] are proposed and are applied in different scenario, among which, L-shaped ULA attracts wide concerns due to its simple structure and ease of implementation. Accordingly, researchers developed numerous methods for estimation of 2-D DOA based on L-shaped ULAs [10–24]. These methods are roughly categorized into two classes: one class is to decouple L-shaped ULA into two separate ULAs, where azimuths and elevations are estimated independently, and the additional 2-D DOA pairing procedure is needed. The other class developed the Vandermonde structure of steering matrix with automatic angles pairing, such as JSVD [18], 2-D MUSIC [20], 2-D PM, 2-D ESPRIT, and their variants [23, 25], of tensor techniques, such as PARAFAC [26], CS-PARAFAC [27], and the tensor-based PARAFAC [8]. Compared to other methods, JSVD and 2-D MUSIC can obtain better angle estimation performance at the expense of prohibitive complexity. Alternatively, the 2-D ESPRIT and 2-D PM show average performance with a moderate or low complexity, but the PARAFAC and CS-PARAFAC methods possess high complexity, thanks to numerous matrix calculations involved, and may converge slowly or even divergent under the case of low signal-to-noise ratio (SNR).

1.1. Our Contributions and Comparisons to Related Work. In order to achieve good estimation performance with automatic angles pairing at the cost of a low or moderate complexity, the conjugate symmetry property of L-shaped ULA is introduced to enlarge virtual array aperture [12]. Motivated by this work, we further generalize virtual aperture by developing not only the forward but also the backward potential rotational invariance property of samples' cross-correlation matrix. As a result, a larger virtual received data matrix is constructed by concatenating the sub-cross-correlation matrices along the columns, and hence, two one-dimensional ESPRITs are constructed to obtain favorable azimuth estimate performance. The proposed methods demonstrate the performance gain as the number of snapshots and of subarray elements increase.

Two kinds of approaches to estimating 2-D DOA are in this paper developed based on the full and partial generalized virtual received data model. One is called the subspace-like method, where the generalization version of PM-ESPRIT algorithm [12] is carried out at a low complexity. The other kind of approach is referred to as the sparse reconstruction method, in which two data models are used to reconstruct sparse 2-D DOA via the M-FOCUSS framework [28] with and without compressive sensing (CS) involvements. We provide a lemma to verify that the received data model is equivalent to its dictionary-based sparse representation; the uniqueness of solutions is guaranteed by assuming azimuth and elevation indices to lie on different rows and columns of sparse signal cross-correlation matrix. In order to demodulate the sparse 2-D DOA, the 2-D MMVs (two-dimensional multiple measurement vectors) are converted into one 1-D MMV and K 1-D SMV (one-dimensional single measurement vector) problems, respectively; the CS-based sparse reconstruction methods are also developed in this paper.

The main contributions of our work are summarized as follows:

(1) We maximize the virtual array aperture of the received data model compared to other existing methods, which greatly benefits 2-D DOA estimation.

(2) We propose an efficient 2-D DOA estimation algorithm for L-shaped array, referred to as the subspace-like method, which outperforms existing methods with a low complexity.

(3) We propose the sparse reconstruction methods with and without CS involvement to estimate 2-D DOA. Particularly, it provides a general framework to estimate 2-D DOA for any array geometry.

1.2. Paper Organization and Notations. The rest of the paper is organized as follows. Section 2 describes the signal model of L-shaped ULA. Section 3 presents two kinds of 2-D DOA estimation approaches based on the full and partial generalized data model. The simulation results and analysis are provided in Section 4. Finally, conclusions are drawn in Section 5.

Throughout the paper, matrices and vectors are denoted by bold capitals and bold lowercases, respectively. $(\cdot)^*$, $(\cdot)^T$, $(\cdot)^{-1}$, $(\cdot)^\dagger$, and $(\cdot)^H$ represent conjugation, transpose, inverse, pseudoinverse, and Hermitian transpose, respectively. $E\{\cdot\}$ denotes the expectation operation. $\odot, \otimes, \mathbf{I}_p, \mathbf{J}_p$, and $\mathbf{O}_{m\times n}$ denote Hadamard product, Kronecker product, $p \times p$ identity matrix, $p \times p$ exchange matrix with ones on antidiagonal and zeros elsewhere, $m \times n$ zero matrix, respectively, $\text{phase}(\cdot)$ and $\text{diag}(\cdot)$ denote, respectively, the phase of its argument and the diagonalization on a vector. $\mathbf{1}_n$ denotes all one vector of size $n \times 1$, and $\text{rank}(\cdot)$ denotes the rank of matrix.

2. Signal Model

As shown in Figure 1, suppose that there are K uncorrelated narrow-band sources (noncircular and/or circular) in far-field impinging upon the L-shaped ULA from directions (θ_k, φ_k), $k = 1, 2, \ldots, K$ (note that here the azimuth definition is different from the traditional one, it is commonly defined with L-shaped array [12, 29]). The L-shaped ULA consists of two orthogonal X-subarray and Z-subarray with each one being M elements, and they share the reference element placed at the origin. The interelement spacing $d = \lambda/2$ for each subarray, where λ is the wavelength of the incident sources.

Let the $M \times 1$ and $(M-1) \times 1$ data vectors received at the t^{th} time of X-subarray and Z-subarray be $\mathbf{x}(t) = [x_1(t), x_2(t), \ldots, x_M(t)]^T$ and $\mathbf{z}(t) = [z_2(t), z_3(t), \ldots, z_M(t)]^T$, respectively. The received data vectors from two subarrays can be written as

$$\begin{aligned} \mathbf{x}(t) &= \mathbf{A}_x(\theta)s(t) + \mathbf{q}_x(t), \\ \mathbf{z}(t) &= \mathbf{A}_z(\varphi)s(t) + \mathbf{q}_z(t), \end{aligned} \tag{1}$$

where $\mathbf{A}_x(\theta)$ and $\mathbf{A}_x(\theta)$ are steering matrices of X-subarray and Z-subarray, respectively.

$$\mathbf{A}_x(\theta) = [\mathbf{a}_x(\theta_1), \mathbf{a}_x(\theta_2), \ldots, \mathbf{a}_x(\theta_K)], \tag{2}$$

$$\mathbf{a}_x(\theta_k) = \left(1, \mu_k, \mu_k^2, \ldots, \mu_k^{M-1}\right)^T, \quad k = 1, \ldots, K, \tag{3}$$

$$\mu_k = \exp\left(\frac{j2\pi d \cos\theta_k}{\lambda}\right), \tag{4}$$

$$\mathbf{A}_z(\varphi) = [\mathbf{a}_z(\varphi_1), \mathbf{a}_z(\varphi_2), \ldots, \mathbf{a}_z(\varphi_K)], \tag{5}$$

$$\mathbf{a}_z(\varphi_k) = \left(\eta_k, \eta_k^2, \ldots, \eta_k^{M-1}\right)^T, \quad k = 1, \ldots, K, \tag{6}$$

$$\eta_k = \exp\left(\frac{j2\pi d \cos\varphi_k}{\lambda}\right), \tag{7}$$

$\mathbf{s}(t) = [s_1(t), s_2(t), \ldots, s_K(t)]^T$ is the received signal vector; $\mathbf{q}_x(t) = [q_{x,1}(t), q_{x,2}(t), \ldots, q_{x,M}(t)]^T$ and $\mathbf{q}_z(t) = [q_{z,1}(t), q_{z,2}(t), \ldots, q_{z,M-1}(t)]^T$ are Gaussian noise vectors of two subarrays, respectively. The additive white Gaussian noise (AWGN) is temporally and spatially independently with

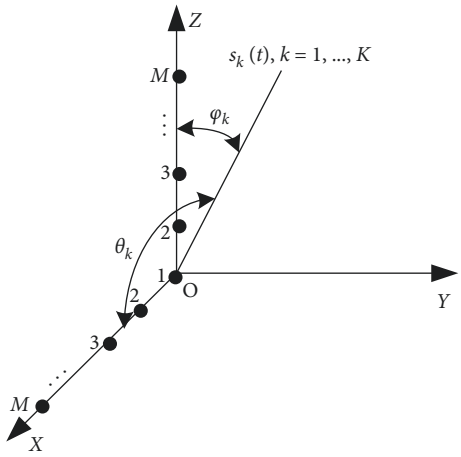

Figure 1: L-shaped ULA geometry.

zero mean and variance σ_n^2 and is uncorrelated with the impinging sources. The highest order in (6) should be $M-1$ since both X-subarray and Z-subarray share the reference element placed at the origin.

3. The Proposed Methods

3.1. Generalized Virtual Aperture Extension Technology. We note that both $\mathbf{A}_x(\theta)$ and $\mathbf{A}_z(\varphi)$ are Vandermonde structure-based steering matrices of centrosymmetric arrays and, therefore, satisfying [23, 30, 31].

$$\mathbf{J}_M \mathbf{A}_x(\theta)^* = \mathbf{A}_x(\theta)\boldsymbol{\Lambda}_x^{-(M-1)}, \tag{8}$$

$$\mathbf{A}_x(\theta)^T \mathbf{J}_M = \boldsymbol{\Lambda}_x^{(M-1)} \mathbf{A}_x(\theta)^H, \tag{9}$$

$$\mathbf{J}_{M-1} \mathbf{A}_z(\varphi)^* = \mathbf{A}_z(\varphi)\boldsymbol{\Lambda}_z^{-M}, \tag{10}$$

$$\mathbf{A}_z(\varphi)^T \mathbf{J}_{M-1} = \boldsymbol{\Lambda}_z^{M} \mathbf{A}_z(\varphi)^H, \tag{11}$$

where $\boldsymbol{\Lambda}_x = \mathrm{diag}(\mu_1, \ldots, \mu_K)$ and $\boldsymbol{\Lambda}_z = \mathrm{diag}(\eta_1, \ldots, \eta_K)$ are two $K \times K$ diagonal matrices containing K azimuth angles $\{\theta_k\}_{k=1}^K$ and K elevation angles $\{\varphi_k\}_{k=1}^K$, respectively. A similar observation has been reported in [12], where only the Vandermonde structure of $\mathbf{A}_z(\varphi)$ is exploited. We instead exploit the Vandermonde structures of both $\mathbf{A}_x(\theta)$ and $\mathbf{A}_z(\varphi)$ and, hence, yields a larger data matrix by generalized virtual aperture extension technology. Our method is stated as follows:

Collect J snapshots for L-shaped ULA; the samples cross-correlation matrix $\widehat{\mathbf{R}}_{x,z}$ of $\mathbf{x}(t)$ and $\mathbf{z}(t)$ is defined by

$$\widehat{\mathbf{R}}_{x,z} \approx E\left\{\mathbf{x}(t)\mathbf{z}(t)^H\right\} = \frac{\mathbf{X}\mathbf{Z}^H}{J} = \mathbf{A}_x(\theta)\widehat{\mathbf{R}}_s \mathbf{A}_z(\varphi)^H, \tag{12}$$

where $\widehat{\mathbf{R}}_s = E\left\{\mathbf{s}(t)\mathbf{s}(t)^H\right\} = \mathrm{diag}(\sigma_1^2, \sigma_2^2, \ldots, \sigma_K^2)$ and σ_k^2 is the received power of the k^{th} source. The estimate of $\widehat{\mathbf{R}}_{x,z}$ is dependent on snapshots J. Defining two selection matrices $\boldsymbol{\psi}_x^{(j)} = [\mathbf{O}_{(M-1)\times(j-1)}, \mathbf{I}_{M-1}, \mathbf{O}_{(M-1)\times(2-j)}]$, $j = 1, 2$, and $\boldsymbol{\psi}_z^{(j)} = [\mathbf{O}_{(M-2)\times(j-1)}, \mathbf{I}_{M-2}, \mathbf{O}_{(M-2)\times(2-j)}]$, $j = 1, 2$, we divide $\widehat{\mathbf{R}}_{x,z}$ into four maximum overlapping submatrices with the size $(M-1)\times(M-2)$, which are denoted by

$$\mathbf{Y}_1 = \boldsymbol{\psi}_x^{(1)} \widehat{\mathbf{R}}_{x,z} \left(\boldsymbol{\psi}_z^{(1)}\right)^T = \mathbf{A}_{x1}(\theta)\widehat{\mathbf{R}}_s \mathbf{A}_{z1}(\varphi)^H, \tag{13}$$

$$\mathbf{Y}_2 = \boldsymbol{\psi}_x^{(1)} \widehat{\mathbf{R}}_{x,z} \left(\boldsymbol{\psi}_z^{(2)}\right)^T = \mathbf{A}_{x1}(\theta)\widehat{\mathbf{R}}_s \mathbf{A}_{z2}(\varphi)^H, \tag{14}$$

$$\mathbf{Y}_3 = \boldsymbol{\psi}_x^{(2)} \widehat{\mathbf{R}}_{x,z} \left(\boldsymbol{\psi}_z^{(1)}\right)^T = \mathbf{A}_{x2}(\theta)\widehat{\mathbf{R}}_s \mathbf{A}_{z1}(\varphi)^H, \tag{15}$$

$$\mathbf{Y}_4 = \boldsymbol{\psi}_x^{(2)} \widehat{\mathbf{R}}_{x,z} \left(\boldsymbol{\psi}_z^{(2)}\right)^T = \mathbf{A}_{x2}(\theta)\widehat{\mathbf{R}}_s \mathbf{A}_{z2}(\varphi)^H, \tag{16}$$

where $\mathbf{A}_{x1}(\theta)$ are the first $M-1$ rows of $\mathbf{A}_x(\theta)$; $\mathbf{A}_{z1}(\varphi)$ are the first $M-2$ rows of $\mathbf{A}_z(\varphi)$; $\mathbf{A}_{x2}(\theta)$ are the last $M-1$ rows of $\mathbf{A}_x(\theta)$; and $\mathbf{A}_{z2}(\varphi)$ are the last $M-2$ rows of $\mathbf{A}_z(\varphi)$; consequently,

$$\begin{aligned} \mathbf{A}_{x2}(\theta) &= \mathbf{A}_{x1}(\theta)\boldsymbol{\Lambda}_x, \\ \mathbf{A}_{z2}(\varphi) &= \mathbf{A}_{z1}(\varphi)\boldsymbol{\Lambda}_z. \end{aligned} \tag{17}$$

As a result, $\mathbf{Y}_2, \mathbf{Y}_3$, and $\mathbf{Y}_4$ in (14)–(16) can be, respectively, rewritten as

$$\begin{aligned} \mathbf{Y}_2 &= \mathbf{A}_{x1}(\theta)\boldsymbol{\Lambda}_z^{-1}\widehat{\mathbf{R}}_s \mathbf{A}_{z1}(\varphi)^H, \\ \mathbf{Y}_3 &= \mathbf{A}_{x1}(\theta)\boldsymbol{\Lambda}_x\widehat{\mathbf{R}}_s \mathbf{A}_{z1}(\varphi)^H, \\ \mathbf{Y}_4 &= \mathbf{A}_{x1}(\theta)\boldsymbol{\Lambda}_x\boldsymbol{\Lambda}_z^{-1}\widehat{\mathbf{R}}_s \mathbf{A}_{z1}(\varphi)^H. \end{aligned} \tag{18}$$

Using the conjugate symmetric properties in (8)–(11) and $\widehat{\mathbf{R}}_s = \widehat{\mathbf{R}}_s^*$, the additional four augmented virtual matrices are yielded

$$\begin{aligned} \mathbf{Y}_5 &= \mathbf{J}_{M-1}\mathbf{Y}_2^*\mathbf{J}_{M-2} = \mathbf{A}_{x1}(\theta)\boldsymbol{\Lambda}_x^{-(M-2)}\boldsymbol{\Lambda}_z^{M}\widehat{\mathbf{R}}_s \mathbf{A}_{z1}(\varphi)^H, \\ \mathbf{Y}_6 &= \mathbf{J}_{M-1}\mathbf{Y}_1^*\mathbf{J}_{M-2} = \mathbf{A}_{x1}(\theta)\boldsymbol{\Lambda}_x^{-(M-2)}\boldsymbol{\Lambda}_z^{(M-1)}\widehat{\mathbf{R}}_s \mathbf{A}_{z1}(\varphi)^H, \\ \mathbf{Y}_7 &= \mathbf{J}_{M-1}\mathbf{Y}_4^*\mathbf{J}_{M-2} = \mathbf{A}_{x1}(\theta)\boldsymbol{\Lambda}_x^{-(M-1)}\boldsymbol{\Lambda}_z^{M}\widehat{\mathbf{R}}_s \mathbf{A}_{z1}(\varphi)^H, \\ \mathbf{Y}_8 &= \mathbf{J}_{M-1}\mathbf{Y}_3^*\mathbf{J}_{M-2} = \mathbf{A}_{x1}(\theta)\boldsymbol{\Lambda}_x^{-(M-1)}\boldsymbol{\Lambda}_z^{(M-1)}\widehat{\mathbf{R}}_s \mathbf{A}_{z1}(\varphi)^H. \end{aligned} \tag{19}$$

Consider a generalized virtual received data model $\mathbf{Y}$ consisting of concatenating $\mathbf{Y}_1 \sim \mathbf{Y}_8$ along the columns, which is denoted by

$$\mathbf{Y} = \left[\mathbf{Y}_1^T, \mathbf{Y}_2^T, \mathbf{Y}_3^T, \mathbf{Y}_4^T, \mathbf{Y}_5^T, \mathbf{Y}_6^T, \mathbf{Y}_7^T, \mathbf{Y}_8^T\right]^T = \mathbf{A}_{xz-\mathrm{aug}}(\theta, \varphi)\widehat{\mathbf{R}}_s \mathbf{A}_{z1}(\varphi)^H, \tag{20}$$

where

$$\mathbf{A}_{xz-\mathrm{aug}}(\theta, \varphi) = \begin{bmatrix} \mathbf{A}_{x1}(\theta) \\ \mathbf{A}_{x1}(\theta)\boldsymbol{\Lambda}_z^{-1} \\ \mathbf{A}_{x1}(\theta)\boldsymbol{\Lambda}_x \\ \mathbf{A}_{x1}(\theta)\boldsymbol{\Lambda}_x\boldsymbol{\Lambda}_z^{-1} \\ \mathbf{A}_{x1}(\theta)\boldsymbol{\Lambda}_x^{-(M-2)}\boldsymbol{\Lambda}_z^{M} \\ \mathbf{A}_{x1}(\theta)\boldsymbol{\Lambda}_x^{-(M-2)}\boldsymbol{\Lambda}_z^{(M-1)} \\ \mathbf{A}_{x1}(\theta)\boldsymbol{\Lambda}_x^{-(M-1)}\boldsymbol{\Lambda}_z^{M} \\ \mathbf{A}_{x1}(\theta)\boldsymbol{\Lambda}_x^{-(M-1)}\boldsymbol{\Lambda}_z^{-(M-1)} \end{bmatrix}, \tag{21}$$

is the generalized steering matrix of size $8(M-1)\times K$; in other words, the effective array aperture is extended significantly, which will substantially improve the azimuth estimation performance, while the elevation estimation will not benefit from the generalized virtual aperture extensive technology. However, we can compromise on the performance between azimuth and elevation flexibly by concatenating $\mathbf{Y}_1 \sim \mathbf{Y}_8$ in other ways.

To estimate 2-D DOA using the generalized virtual received data model $\mathbf{Y}$ in (20), we propose two kinds of methods, i.e., the subspace-like method and the sparse reconstruction method, which are formulated in a way that no angles pairing issue arises.

3.2. The Subspace-Like Method. One effective method to obtain $\{(\theta_k, \varphi_k)\}_{k=1}^K$ is to apply generalization of PM-ESPRIT algorithm [12] (Section 3) to the generalized steering matrix (21). We can find propagator matrix by using PM, which partitions $\mathbf{A}_{xz-\text{aug}}(\theta,\varphi)$ into two submatrices $\mathbf{A}_{xz-1}(\theta,\varphi)$ and $\mathbf{A}_{xz-2}(\theta,\varphi)$ of size $K\times K$ and $(8(M-1)-K)\times K$, respectively.

$$\mathbf{A}_{xz-\text{aug}}(\theta,\varphi) = \left[\, \mathbf{A}_{xz-1}(\theta,\varphi)^T \;\; \mathbf{A}_{xz-2}(\theta,\varphi)^T \right]^T. \tag{22}$$

Under the hypothesis that $\mathbf{A}_{xz-1}(\theta,\varphi)$ is a nonsingular matrix (which is sufficient for subspace-like methods while $M-1\geq K$), the propagator matrix $\mathbf{P}$ is a unique linear operator, which satisfies

$$\mathbf{P}^H \mathbf{A}_{xz-1}(\theta,\varphi) = \mathbf{A}_{xz-2}(\theta,\varphi). \tag{23}$$

By solving a LS problem, $\mathbf{P}$ is achieved by

$$\widehat{\mathbf{P}} = \left(\widetilde{\mathbf{Y}}_1 \widetilde{\mathbf{Y}}_1^{\,H}\right)^{-1} \widetilde{Y}_1 \widetilde{Y}_2^H, \tag{24}$$

where $\mathbf{Y} = [\widetilde{Y}_1^T, \widetilde{Y}_2^T]^T$ and $\widetilde{\mathbf{Y}}_1 \in C^{K\times(M-2)}$, $\widetilde{\mathbf{Y}}_2 \in C^{(8(M-1)-K)\times(M-2)}$. Let $\mathbf{Q} = \begin{bmatrix} \mathbf{I}_K \\ \widehat{\mathbf{P}}^H \end{bmatrix}$ denotes an extended propagator matrix; we have $\mathbf{Q}\mathbf{A}_{xz-1}(\theta,\varphi) = \mathbf{A}_{xz-\text{aug}}(\theta,\varphi)$. Define two azimuth angle selection matrices as follows

$$\Upsilon_x^{(j)} = \mathbf{I}_8 \otimes \left[\mathbf{O}_{(M-2)\times(j-1)}, \mathbf{I}_{M-2}, \mathbf{O}_{(M-2)\times(2-j)}\right], \quad j = 1, 2. \tag{25}$$

We observe that the rotational invariance property of $\mathbf{A}_{xz-\text{aug}}(\theta,\varphi)$ still holds, and hence,

$$\Upsilon_x^{(1)} \mathbf{Q}\mathbf{A}_{xz-1}(\theta,\varphi)\mathbf{\Lambda}_x = \Upsilon_x^{(2)} \mathbf{Q}\mathbf{A}_{xz-1}(\theta,\varphi). \tag{26}$$

By carrying out simple operations to (26), a new $K\times K$ nonsingular matrix T_x is achieved

$$\mathbf{T}_x = \left(\Upsilon_x^{(1)}\mathbf{Q}\right)^{\dagger}\left(\Upsilon_x^{(2)}\mathbf{Q}\right) = \mathbf{A}_{xz-1}(\theta,\varphi)\mathbf{\Lambda}_x\mathbf{A}_{xz-1}(\theta,\varphi)^{-1}. \tag{27}$$

Applying eigenvalue decomposition (EVD) to T_x, the estimation of $\mathbf{\Lambda}_x$ can be written as $\widehat{\mathbf{\Lambda}}_x = \mathbf{\Delta}\mathbf{\Lambda}_x\mathbf{\Delta}$, where $\mathbf{\Delta}$ is the $K\times K$ permutation matrix satisfying $\mathbf{\Delta}^T = \mathbf{\Delta}^{-1}$. Let $\widehat{\mathbf{A}}_{xz-1}(\theta,\varphi)$ denotes the estimation of $\mathbf{A}_{xz-1}(\theta,\varphi)$; we have $\widehat{\mathbf{A}}_{xz-1}(\theta,\varphi) = \mathbf{A}_{xz-1}(\theta,\varphi)\mathbf{\Delta}$. Note that the scaling ambiguity is not considered here since $\mathbf{\Lambda}_x$ is unitary matrix and its diagonal elements locate on the unit circle.

In order to achieve 2-D DOA automatic pairing, let $\Upsilon_z^{(j)}$, $j = 1, 2$ be two elevation angle selection matrices, which is defined as

$$\Upsilon_z^{(j)} = \mathbf{I}_4 \otimes \left[\mathbf{O}_{(M-1)\times((j-1)(M-1))}, \mathbf{I}_{M-1}, \mathbf{O}_{(M-1)\times((2-j)(M-1))}\right]. \tag{28}$$

Again by utilizing the rotational invariance property of $\mathbf{A}_{xz-\text{aug}}(\theta,\varphi)$ used in (26) and substitute $\mathbf{A}_{xz-1}(\theta,\varphi)$ with $\widehat{\mathbf{A}}_{xz-1}(\theta,\varphi)$, we have

$$\Upsilon_z^{(1)}\mathbf{Q}\widehat{\mathbf{A}}_{xz-1}(\theta,\varphi)\mathbf{\Delta}\mathbf{\Lambda}_z^{-1} = \Upsilon_z^{(2)}\mathbf{Q}\widehat{\mathbf{A}}_{xz-1}(\theta,\varphi)\mathbf{\Delta}. \tag{29}$$

Left-multiply and right-multiply both sides of (29) by $(\Upsilon_z^{(2)}\mathbf{Q}\widehat{\mathbf{A}}_{xz-1}(\theta,\varphi))^{\dagger}$ and $\mathbf{\Lambda}_z\mathbf{\Delta}$, respectively; the estimation $\widehat{\mathbf{\Lambda}}_z$ is denoted as

$$\widehat{\mathbf{\Lambda}}_z = \mathbf{\Delta}\mathbf{\Lambda}_z\mathbf{\Delta} = \left(\Upsilon_z^{(2)}\mathbf{Q}\widehat{\mathbf{A}}_{xz-1}(\theta,\varphi)\right)^{\dagger}\left(\Upsilon_z^{(1)}\mathbf{Q}\widehat{\mathbf{A}}_{xz-1}(\theta,\varphi)\right). \tag{30}$$

The angle pairing is achieved automatically via $\widehat{\mathbf{A}}_{xz-1}(\theta,\varphi)$, which associates $\widehat{\mathbf{\Lambda}}_x$ with $\widehat{\mathbf{\Lambda}}_z$ without permutation ambiguity. Therefore, the estimates of $\{(\theta_k,\varphi_k)\}_{k=1}^K$ can be obtained by

$$\begin{aligned} \left\{\widehat{\theta}_k\right\}_{k=1}^K &= \arccos\left(\frac{\text{phase}\left(\widehat{\mathbf{\Lambda}}_x\right)\cdot\lambda}{(2\pi d)}\right), \\ \left\{\widehat{\varphi}_k\right\}_{k=1}^K &= \arccos\left(\frac{\text{phase}\left(\widehat{\mathbf{\Lambda}}_z\right)\cdot\lambda}{(2\pi d)}\right). \end{aligned} \tag{31}$$

Note: the azimuth angle estimation utilizes the rotational invariance property from two $8(M-1)$ element data, while the elevation estimation only use the rotational invariance property from two $4(M-1)$ element data; in such case, the azimuth estimation performance is better than that of elevation.

The main steps of the proposed subspace-like method are summarized as follows:

(1) Calculate the extended propagator matrix via the generalized steering matrix.

(2) Develop the rotational invariance property of the generalized steering matrix $\mathbf{A}_{xz-\text{aug}}(\theta,\varphi)$ to obtain a nonsingular matrix T_x via two azimuth angle selection matrices.

(3) Apply eigenvalue decomposition to T_x, and the estimations of eigenvalue matrix $\mathbf{\Lambda}_x$ and eigenvector matrix $\mathbf{A}_{xz-1}(\theta,\varphi)$ are obtained; the azimuths are estimated from $\widehat{\mathbf{\Lambda}}_x$.

(4) Develop the rotational invariance property of the generalized steering matrix $\mathbf{A}_{xz-\text{aug}}(\theta,\varphi)$ but replace $\mathbf{A}_{xz-1}(\theta,\varphi)$ with $\widehat{\mathbf{A}}_{xz-1}(\theta,\varphi)$ estimated from step 3,

the autopaired elevation estimation is achieved via two elevation angle selection matrices.

3.3. The Sparsity Reconstruction Method. Assume that 2-D DOA search ranges are divided into N_θ and N_φ angle grids denoted by θ_p, $p = 1, 2, \ldots, N_\theta$, and φ_q, $q = 1, 2, \ldots, N_\varphi$, respectively. Define in the spatial domain two basis matrices $\mathbf{\Omega}_\theta$ of size $M \times N_\theta$, $N_\theta \gg M$ and $\mathbf{\Omega}_\varphi$ of size $(M-1) \times N_\varphi$, $N_\varphi \gg M - 1$ as

$$\begin{aligned}
\mathbf{\Omega}_\theta &= \left[\boldsymbol{\eta}_\theta(\theta_1), \boldsymbol{\eta}_\theta(\theta_2), \ldots, \boldsymbol{\eta}_\theta\left(\theta_{N_\theta}\right)\right], \\
\boldsymbol{\eta}_\theta\left(\theta_p\right) &= \frac{\left(1, e^{j2\pi d \cos\theta_p/\lambda}, \ldots, e^{j2\pi(M-1)d\cos\theta_p/\lambda}\right)^T}{\sqrt{M}}, \\
\mathbf{\Omega}_\varphi &= \left[\boldsymbol{\eta}_\varphi(\varphi_1), \boldsymbol{\eta}_\varphi(\varphi_2), \ldots, \boldsymbol{\eta}_\varphi\left(\varphi_{N_\varphi}\right)\right], \\
\boldsymbol{\eta}_\varphi\left(\varphi_q\right) &= \frac{\left(e^{j2\pi d \cos\theta_q/\lambda}, \ldots, e^{j2\pi(M-1)d\cos\theta_q/\lambda}\right)^T}{\sqrt{M-1}},
\end{aligned} \tag{32}$$

where $p = 1, \ldots, N_\theta$, $q = 1, \ldots, N_\varphi$; $\boldsymbol{\eta}_\theta(\theta_p)$ and $\boldsymbol{\eta}_\varphi(\varphi_q)$ are the array steering basis vectors of θ_p and φ_q, respectively. Suppose the pairing $\{(\theta_k, \varphi_k)\}_{k=1}^K$ of K sources just fall on the 2-D DOA angle grids and indexed by $\{(p_k, q_k)\}_{k=1}^K$, respectively. Taking the samples cross-correlation matrix (12) into account, we can recast (12) into the dictionary-based sparse representation

$$\widehat{\mathbf{R}}_{x,z} = \mathbf{A}_x(\theta)\widehat{\mathbf{R}}_s\mathbf{A}_z(\varphi)^H = \mathbf{\Omega}_\theta\mathbf{\Theta}_s\mathbf{\Omega}_\varphi^H, \tag{33}$$

where $\mathbf{\Theta}_s$ is a $N_\theta \times N_\varphi$ sparse matrix containing only K nonzero coefficients, i.e., $\mathbf{\Theta}_s(p_k, q_k) = \sigma_k^2$; the similar observation is achieved in [32], wherein it is only studied numerically without theoretical analysis. The following lemma proves that equation (33) holds subject to certain mild constraints on the basis matrices and the sources.

Lemma 1. *Considering (33) with the assumptions that any M columns of $\mathbf{\Omega}_\theta$ and any $M-1$ columns of $\mathbf{\Omega}_\varphi$ are linearly independent, the received signals are uncorrelated and independently across the array which ensures $rank(\mathbf{\Omega}_\theta) = M$ and $rank(\mathbf{\Omega}_\varphi) = M - 1$; the columns of basis matrices $\mathbf{\Omega}_\theta$ and $\mathbf{\Omega}_\varphi$ are not nearly collinear to the columns that form the basis for the $\mathbf{\Theta}_s$, which guarantee the uniqueness of solutions, but to what extent depends on the signal-to-noise ratio (SNR) and angular interval between the columns of $\mathbf{\Omega}_\theta$ and $\mathbf{\Omega}_\varphi$, if $rank(\mathbf{\Theta}_s) = K \le M - 1$, i.e., $p_i \ne p_j, q_i \ne q_j, i \ne j$, then $\mathrm{rank}(\mathbf{Y}_1) = K$, and (33) is satisfied.*

Proof. From the assumptions above, we have $\mathrm{rank}(\mathbf{\Omega}_\theta) = M$, $\mathrm{rank}(\mathbf{\Theta}_s) = K$, and $\mathrm{rank}(\mathbf{\Omega}_\varphi) = M - 1$. Therefore, $\mathrm{rank}(\mathbf{\Theta}_s\mathbf{\Omega}_\varphi^H) \le \min\{\mathrm{rank}(\mathbf{\Theta}_s), \mathrm{rank}(\mathbf{\Omega}_\varphi)\} = K$. Let $\mathbf{Z} = \mathbf{\Omega}_\theta\mathbf{\Theta}_s\mathbf{\Omega}_\varphi^H$, $\mathrm{rank}(\mathrm{Z}) = \mathrm{rank}(\mathbf{\Omega}_\theta\mathbf{\Theta}_s\mathbf{\Omega}_\varphi^H) \le \min\{\mathrm{rank}(\mathbf{\Omega}_\theta), \mathrm{rank}(\mathbf{\Theta}_s\mathbf{\Omega}_\varphi^H)\} = K$. Without loss of generality, we assume that the first K rows and the first K columns of Θ_s (the case where those linear independent columns are dispersed randomly across the matrix $\mathbf{\Theta}_s$ can be dealt in a similar manner) are linearly independently, yielding a new matrix $\mathbf{T}_s$, which is equivalent to $\widehat{\mathbf{R}}_s$, i.e., $\mathbf{\Gamma}_s = \Xi\widehat{\mathbf{R}}_s\Xi$. Accordingly, the generating matrices $\widetilde{\mathbf{\Omega}}_\theta$ and $\widetilde{\mathbf{\Omega}}_\varphi^H$, consisting of the first K columns of $\mathbf{\Omega}_\theta$ and the first K rows of $\mathbf{\Omega}_\varphi^H$, are intrinsically equivalent matrices of $\mathbf{A}_{x1}(\theta)$ and $\mathbf{A}_{z1}(\varphi)^H$, respectively; that is to say $\widetilde{\mathbf{\Omega}}_\theta = \mathbf{A}_{x1}(\theta)\Xi$ and $\widetilde{\mathbf{\Omega}}_\varphi = \mathbf{A}_{z1}(\varphi)\Xi$; Ξ is the $K \times K$ permutation matrix satisfying $\Xi^T = \Xi^{-1}$. As a result, $\mathbf{\Omega}_\theta\mathbf{\Theta}_s\mathbf{\Omega}_\varphi^H = \widetilde{\mathbf{\Omega}}_\theta\mathbf{\Gamma}_s\widetilde{\mathbf{\Omega}}_\varphi^H$, $\widetilde{\mathbf{\Omega}}_\theta\mathbf{\Gamma}_s\widetilde{\mathbf{\Omega}}_\varphi^H = \mathbf{A}_{x1}(\theta)\Xi\Xi\widehat{\mathbf{R}}_\mathbf{s}\Xi\Xi\mathbf{A}_{z1}(\varphi)^H = \mathbf{A}_{x1}(\theta)\widehat{\mathbf{R}}_\mathbf{s}\mathbf{A}_{z1}(\varphi)^H$; therefore, $\mathbf{Y}_1 = \mathbf{A}_{x1}(\theta)\widehat{\mathbf{R}}_\mathbf{s}\mathbf{A}_{z1}(\varphi)^H = \mathbf{\Omega}_\theta\mathbf{\Theta}_s\mathbf{\Omega}_\varphi^H$, $\mathrm{rank}(\mathbf{Y}_1) = K$, we complete the proof. Lemma 1 associates the parameter-based data models with its sparse representations.

The multiple measurement vector (MMV) sparse reconstruction is first addressed in [28], which is used to compute the sparse solutions given MMV that shares a common sparsity structure, wherein it exploits the sparsity in angle domain. Later, [32] extends 1-D MMV to 2-D MMV. In this context, the 2-D DOA sparse reconstruction is derived, and the sparse solutions are reconstructed via the M-FOCUSS [28] with and without the involvements of CS based on two received data models.

3.3.1. On the Data Model (33) with and without CS Involvements. First, we make use of (33) as the data model. In order to estimate $\mathbf{\Theta}_s$, we set up the cost function as follows:

$$\begin{aligned}
\mathrm{Z}_{\theta,\varphi}^* &= \arg\min_{\mathrm{Z}_{\theta,\varphi}} \left\|\mathrm{Z}_{\theta,\varphi}\right\|_{2,s}, \\
\text{s.t. } \widehat{\mathbf{R}}_{x,z} &= \mathbf{\Omega}_\theta\mathrm{Z}_{\theta,\varphi},
\end{aligned} \tag{34}$$

where $\mathrm{Z}_{\theta,\varphi} = \mathbf{\Theta}_s\mathbf{\Omega}_\varphi^H$, $\|\mathrm{Z}_{\theta,\varphi}\|_{2,s} \triangleq \sum_{r=1}^{N_\theta}(\|\mathbf{z}_r\|_2)^s$, $s \in [0, 1]\mathbf{z}_r = [z_r(1), \ldots, z_r(M-1)]$ is the r^{th} row of $\mathbf{Z}_{\theta,\phi}$, and the row norm is 2-norm defined by $\|\mathbf{z}_r\|_2 = (\sum_{l=1}^{M-1}|z_r(l)|^2)^{1/2}$; $M-1$ denotes the number of MMVs; N_θ denotes rows vectors of sparse solutions; s is the sparsity measure that balances the performance and the complexity. Equation (34) converts equation (33) 1-D MMV problem, where $\mathrm{Z}_{\theta,\varphi}$ contains only K nonzero rows vector index supports corresponding to azimuth angles $\{\theta_k\}_{k=1}^K$. By letting certain termination condition be satisfied, we take out K nonzero rows with the maximum amplitudes from N_θ rows vectors to form $\mathrm{Z}_{\theta,\varphi}^*$, i.e., $\mathrm{Z}_{\theta,\varphi}^* = \mathbf{\Omega}_{\theta,0}^\dagger\widehat{\mathbf{R}}_{x,z}$, $\mathbf{\Omega}_{\theta,0} = [\boldsymbol{\eta}_\theta(\theta_{n_1}), \boldsymbol{\eta}_\theta(\theta_{n_2}), \ldots, \boldsymbol{\eta}_\theta(\theta_{n_K})]$, $\mathbf{I}_K = \{n_1, n_2, \ldots, n_K\}$ is the rows sparse index supports. In order to estimate elevations $\{\varphi_k\}_{k=1}^K$, we need to solve additional K 1-D SMV problems of

$$\begin{aligned}
\boldsymbol{\theta}_{s,k}^* &= \arg\min_{\boldsymbol{\theta}_{s,k}} \left\|\boldsymbol{\theta}_{s,k}^H\right\|_{2,s}, \\
\text{s.t. } \mathbf{z}_{\theta,\varphi,k}^* H &= \mathbf{\Omega}_\varphi\boldsymbol{\theta}_{s,k}^H,
\end{aligned} \tag{35}$$

where $\mathbf{z}_{\theta,\varphi,k}^*$ is the k^{th} row vector of $\mathrm{Z}_{\theta,\varphi}^*$; $\boldsymbol{\theta}_{s,k}^*$ is the k^{th} row vector of $\mathbf{\Theta}_s$; the k^{th} nonzero coefficient is found from $\boldsymbol{\theta}_{s,k}^*$; the angles pairing is achieved automatically. Note: K

azimuth angles $\{\theta_k\}_{k=1}^{K}$ are first found from K nonzero rows vector index supports at a single time slot, and then K elevation angles $\{\varphi_k\}_{k=1}^{K}$ are found from K different row vectors by K time slots, which implies a fact that small azimuth angle separation will lead to poor azimuth estimation performance, but elevation estimation performance will not be affected even if the elevation angle separation is small.

The proposed methods, inspired by [32], extend 2-D sparse reconstruction methods to CS-based sparse reconstruction in such a way that no angles pairing issue arises. This method allows for recovery of 2-D DOA assuming they stay on the predefined 2-D angle grids.

Define two spatial domain compression matrices $\mathbf{\Phi}_x$ of size $M_l \times M$, $(M_l \le M)$ and $\mathbf{\Phi}_z$ of size $M_k \times (M-1)$, $M_k \le (M-1)$, respectively, whose elements are drawn *i.i.d* from a Gaussian distribution with zero mean and unit variance. Left-multiply $\mathbf{\Phi}_x$ and right-multiply $\mathbf{\Phi}_z^H$ by $\widehat{\mathbf{R}}_{x,z}$, the CS-based samples cross-correlation matrix $\widehat{\mathbf{R}}_{x,z}^{(\mathrm{CS})}$ becomes

$$\widehat{\mathbf{R}}_{x,z}^{(\mathrm{CS})} = \mathbf{\Phi}_x \widehat{\mathbf{R}}_{x,z} \mathbf{\Phi}_z^H = \mathbf{\Phi}_x \mathbf{\Omega}_\theta \mathbf{\Theta}_s \mathbf{\Omega}_\varphi^H \mathbf{\Phi}_z^H = \widetilde{\mathbf{\Omega}}_\theta \mathbf{\Theta}_s \widetilde{\mathbf{\Omega}}_\varphi^H, \quad (36)$$

where $\widetilde{\mathbf{\Omega}}_\theta = \mathbf{\Phi}_x \mathbf{\Omega}_\theta$ and $\widetilde{\mathbf{\Omega}}_\varphi = \mathbf{\Phi}_z \mathbf{\Omega}_\varphi$ are the composite azimuth and elevation angle basis matrices, respectively; the incorporation of compression matrices into the received data matrix will benefit lower storage request. The CS-based sparse reconstruction method is implemented using the same procedures as shown in (34) and (35).

3.3.2. On the Data Model (20) with and without CS Involvements. The new insight into the 2-D sparse reconstruction method can also be obtained by developing the common sparse structure of the partial generalized data model (20), which will improve the azimuth estimation performance even when the azimuth separations are close. From Lemma 1, we know the basis matrix $\mathbf{\Omega}_\theta$ and $\mathbf{\Omega}_\varphi$ must be row full rank and $\mathrm{rank}(\mathbf{\Theta}_s) = K$; hence, we select from $\mathbf{Y}$ in (20) the group $\{\mathbf{Y}_1, \mathbf{Y}_3\}$ to construct a column full rank data matrix $\mathbf{Y}_{13} = (\mathbf{Y}_1{}^T, \widehat{Y}_3{}^T)^T$ of size $M \times (M-2)$, where $\widehat{Y}_3 = \mathbf{e}_{M-1}^T \mathbf{Y}_3$, $\mathbf{e}_{M-1} = [0, \ldots, 0, 1]^T$ is the unit vector of size $M-1$. Taking the Hermitian transpose over $\mathbf{Y}_{13}$, $\mathbf{Y}_{13}^H$ can be represented as

$$\mathbf{Y}_{13}^H = \mathbf{A}_{z1}(\varphi) \widehat{\mathbf{R}}_s^H \mathbf{B}_{x1}(\theta)^H, \quad (37)$$

where $\mathbf{B}_{x1}(\theta)^H = \left[\, \mathbf{A}_{x1}(\theta)^H \;\; \mathbf{\Lambda}_x^H \mathbf{A}_{x1}(\theta)^H \mathbf{e}_{M-1} \,\right]$, from Lemma 1, we recast (37) as

$$\mathbf{Y}_{13}^H = \widetilde{\mathbf{A}}_{z1}(\varphi) \widetilde{\mathbf{R}}_s^H \widetilde{\mathbf{B}}_{x1}(\theta)^H, \quad (38)$$

where $\widetilde{\mathbf{A}}_{z1}(\varphi)$, $\widetilde{\mathbf{R}}_s$, and $\widetilde{\mathbf{B}}_{x1}(\theta)$ are $(M-2) \times N_\varphi$, $N_\theta \times N_\varphi$, and $M \times N_\theta$ basis matrices of $\mathbf{A}_{z1}(\varphi)$, $\widehat{\mathbf{R}}_s$, and $\mathbf{B}_{x1}(\theta)$, respectively. $\widetilde{\mathbf{B}}_{x1}(\theta)^H = \left[\, \widetilde{\mathbf{A}}_{x1}(\theta)^H \;\; \widetilde{\mathbf{\Lambda}}_x^H \widetilde{\mathbf{A}}_{x1}(\theta)^H \mathbf{e}_{M-1} \,\right]$, $\widetilde{\mathbf{\Lambda}}_x = \mathrm{diag}(\mu_1, \mu_2, \ldots, \mu_{N_\theta})$ is $N_\theta \times N_\theta$ diagonal matrix; $\widetilde{\mathbf{A}}_{x1}(\theta)$ is $(M-1) \times N_\theta$ basis matrix of $\mathbf{A}_{x1}(\theta)$. Note: one can also define the groups $\{\mathbf{Y}_2, \mathbf{Y}_4\}, \{\mathbf{Y}_5, \mathbf{Y}_7\}, \{\mathbf{Y}_6, \mathbf{Y}_8\}$ to make new data matrices which provide the similar performance as $\mathbf{Y}_{13}$, but $\mathbf{Y} = \{\mathbf{Y}_1, \ldots, \mathbf{Y}_8\}$ may not provide better performance since the generalized steering basis matrix is rank deficit and does not suffice Lemma 1. Similar to (34), we establish the cost function

$$\begin{aligned} \widetilde{\mathbf{Z}}_{\theta,\varphi}^* &= \arg\min_{\widetilde{\mathbf{Z}}_{\theta,\varphi}} \left\| \widetilde{\mathbf{Z}}_{\theta,\varphi} \right\|_{2,s}, \\ \text{s.t. } \mathbf{Y}_{13}^H &= \widetilde{\mathbf{A}}_{z1}(\varphi) \widetilde{\mathbf{Z}}_{\theta,\varphi}, \end{aligned} \quad (39)$$

where $\widetilde{\mathbf{Z}}_{\theta,\varphi} = \widetilde{\mathbf{R}}_s^H \widetilde{B}_{x1}(\theta)^H$, by enforcing some termination condition to (39), we select out K nonzero rows with the maximum amplitudes to form $\widetilde{\mathbf{Z}}_{\theta,\varphi}^*$, i.e., $\widetilde{\mathbf{Z}}_{\theta,\varphi}^* = \widetilde{\mathbf{A}}_{z1,0}(\varphi)^\dagger \mathbf{Y}_{13}^H$, $\widetilde{\mathbf{A}}_{z1,0}(\varphi) = [\widetilde{\mathbf{A}}_{z1}(\varphi_{m_1}), \widetilde{\mathbf{A}}_{z1}(\varphi_{m_2}), \ldots, \widetilde{\mathbf{A}}_{z1}(\varphi_{m_K})]$, $\mathbf{I}_K = \{m_1, m_2, \ldots, m_K\}$ is the row sparse index supports. Again additional K 1-D SMV problems of

$$\begin{aligned} \widetilde{\mathbf{r}}_{s,k}^* &= \arg\min_{\widetilde{\mathbf{r}}_{s,k}} \left\| \widetilde{\mathbf{r}}_{s,k}^H \right\|_{2,s}, \\ \text{s.t. } \widetilde{\mathbf{z}}_{\theta,\varphi,k}^* H &= \widetilde{\mathbf{B}}_{x1}(\theta) \widetilde{\mathbf{r}}_{s,k}^H, \end{aligned} \quad (40)$$

have to be solved to obtain $\{\theta_k\}_{k=1}^{K}$; the angles pairing is achieved automatically. Note: K elevation angles $\{\theta_k\}_{k=1}^{K}$ are first found from K nonzero rows vector index supports of $\widetilde{Z}_{\theta,\varphi}$ at a single time slot, and then K azimuth angles $\{\theta_k\}_{k=1}^{K}$ are found from K different row vectors at K time slots, which suggests a fact that small elevation separation will yield poor elevation estimation performance, but azimuth estimation performance will not be affected even if the azimuth separations are small.

Define two spatial domain compression matrices $\mathbf{\Phi}_x^{(13)}$ of size $M_l \times M$, $M_l \le M$, and $\mathbf{\Phi}_z^{(13)}$ of size $M_k \times (M-2)$, $M_k \le (M-2)$, whose elements are drawn *i.i.d* from a Gaussian distribution with zero mean and unit variance, respectively. Left-multiply $\mathbf{\Phi}_z^{(13)}$ and right-multiply $\mathbf{\Phi}_x^{(13)H}$ by $\mathbf{Y}_{13}^H$, the CS-based data matrices $\mathbf{Y}_{13}^{(\mathrm{CS})H}$ become

$$\begin{aligned} \mathbf{Y}_{13}^{(\mathrm{CS})H} &= \mathbf{\Phi}_z^{(13)} \mathbf{Y}_{13}^H \mathbf{\Phi}_x^{(13)H} \\ &= \mathbf{\Phi}_x^{(13)} \widetilde{\mathbf{A}}_{z1}(\varphi) \widetilde{\mathbf{R}}_s^H \widetilde{B}_{x1}(\theta)^H \mathbf{\Phi}_x^{(13)H} \\ &= \widetilde{\widetilde{\mathbf{A}}}_{z1}(\varphi) \widetilde{\mathbf{R}}_s^H \widetilde{\widetilde{\mathbf{B}}}_{x1}(\theta)^H, \end{aligned} \quad (41)$$

where $\widetilde{\widetilde{\mathbf{A}}}_{z1}(\varphi) = \mathbf{\Phi}_z^{(13)} \widetilde{\mathbf{A}}_{z1}(\varphi)$ and $\widetilde{\widetilde{\mathbf{B}}}_{x1}(\theta) = \mathbf{\Phi}_x^{(13)} \widetilde{\mathbf{B}}_{x1}(\theta)$ are the composite 2-D DOA basis matrices. The CS-based sparse reconstruction procedure is implemented using the same methods as those in (39) and (40).

The major steps of the sparse reconstruction methods are summarized as follows:

(1) Establish the sparse representation models based on the conventional data model and the partial generalized data model.

(2) Establish cost functions to minimize the errors based on M-FOCUSS framework.

(3) Transform the 2-D DOA estimation into two associated 1-D MMV problems, and the autopaired

angles are achieved by solving the two optimization problems successively.

Remark 1. From (26) and (29), it is obvious that the array aperture, of $\{\theta_k\}_{k=1}^K$ and $\{\varphi_k\}_{k=1}^K$, is enhanced greatly from M to $8(M-1)$ and from M to $4(M-1)$, respectively.

Remark 2. The subspace-like method provides super-resolution when the received data matrix is modeled accurately for the L-shaped array. By contrast, the sparse reconstruction methods do not impose any restricts on the array structure, either nonlinear or nonuniform. On the other hand, the number of the maximum identifiable sparse solutions K [33] should satisfy $K < (M-1)/2$ for two kinds of approaches.

4. Simulation Results and Analysis

4.1. Computational Complexity Analysis. In this subsection, we present the complexity analysis for the competitive methods, the complexity of EAET [12] is $O\{M^2N + 8MK^2 + 4M(4M-K)K + 8(M-1)K^2\}$, of JSVD [18] is $O\{M^2N + 2M(M-1)^2 + 2MK^2 + K^3 + N_sM^2K\}$, of PARAFAC [26] is $O\{4(M-1)^2N + N_{it}[(M-1)^2K^2 + 13(M-1)^2K + 8(M-1)K^2 + 8(M-1)K]\}$, of CSAP [29] is $O\{M^2N + 16M^3 + N_s[16M^2 + 2 + 4M^2(2M-K)]\}$, of AAEA [10] is $O\{M^2N + 9M^3 + 6M^2K + 2MK^3 + 18MK^2 + 3K^3\}$, and of the proposed subspace-like method is $O[M^2N + 2K^2(M-2) + K(M-2)(8(M-1)-K) + 16(M-2)K^2 + 4K^3]$, where N_s, N_{it} denote the total search times within the search range and the number of iteration, respectively. As $N_s \gg M, N_s \gg K$, and $M > K$, the subspace-like method is more computationally efficient than the JSVD and CSAP and is close to AAEA method, the complexity of sparse reconstruction methods depends on the implementation of M-FOCUSS [28]. Meanwhile, it is quite difficult to compare the proposed methods with the PARAFAC method, since the number of iterations depends on heavily the received data and possibly varies dramatically. Therefore, the other complexity benchmark is to numerically compare the CPU runtime of the competitive methods as used, for example, in [12, 29]. In this paper, all simulations are carried out on a laptop configured as follows: MATLAB R2016b, Intel ® Core™ i5-6200U CPU@ 2.30 GHz and 8 GB RAM.

4.2. Simulation and Parameter Settings. Simulations are conducted to evaluate azimuth estimation performances of the proposed approaches in this section, since the array aperture is significantly extended in azimuths but is slightly extended in elevations. The search range of azimuths and elevations is $[0^\circ, 180^\circ]$ with step 0.1° for JSVD [18] and CSAP [29]. The performance of the proposed subspace-like method is compared with EAET [12], JSVD [18], PARAFAC [26], CSAP [29], AAEA [10], and CRB (Cramer-Rao Bound). The K sources are drawn from the standard normal distribution $\mathbf{s}_k(t) \sim N(0,1)$, $t = 1, \ldots, J$. $I = 500$ is the number of Monte Carlo trials used throughout all simulations, and SNR is defined as $10\log_{10}(\sigma_s^2/\sigma_w^2)$, where σ_s^2, σ_w^2 denote the power of signals and noise, respectively.

4.2.1. 2-D DOA Estimation Performance

Example 1. The 2-D DOA estimation performance of the proposed subspace-like method is compared to EAET [12] in this example. There are in the far-field $K = 3$ uncorrelated narrow-band sources from the directions $(60.25^\circ, 45.39^\circ)$, $(30.88^\circ, 80.19^\circ)$, $(133.05^\circ, 160.60^\circ)$ impinging on the L-shaped ULA. Both $M = 7$ and $J = 500$ are fixed. We set SNR = 20 dB and run $I = 500$ Monte Carlo trials to observe scatters of 2-D DOA estimations.

As shown in Figure 2, we observe that the estimation variance derived by the subspace-like method is smaller than EAET [12] because the proposed method develops generalized virtual aperture.

4.2.2. RMSE vs. SNR for the Subspace-Like Method

Example 2. The performance of the subspace-like method, against SNR varying from −5 dB to 20 dB with interval 2.5 dB, is studied in this example. The sources angles are $(99^\circ, 91^\circ)$, $(100^\circ, 65^\circ)$, and $(101^\circ, 76^\circ)$; the other parameters are the same as those in Example 1. The RMSE of azimuth estimation vs. SNR is shown in Figure 3. As observed in the figure, the azimuth estimation performance for the proposed method is better than other methods because the subspace-like method utilizes the rotational invariance property from two $8(M-1)$ elements array data while EAET [12] only use the rotational invariance property from two $4(M-1)$ elements array data. One of the most significant advantages is the proposed subspace-like method possesses the super-resolution capability.

4.2.3. RMSE vs. Snapshots for the Subspace-Like Method

Example 3. Let SNR = 10 dB be fixed and the number of snapshots varies from 100 to 1000 with step 100; the other parameters are the same as those in Example 2. The RMSE of azimuth estimation versus snapshots is illustrated in Figure 4. Again, we observe that the estimation performance of the proposed method improves as snapshots increase and is the best of all competitive methods, from which we have similar observation and analysis.

4.2.4. RMSE vs. Azimuth Separations for the Subspace-Like Method

Example 4. From the previous examples, we note that the performance of the proposed subspace method is a little higher than that of EAET [12]. In this example, we hope to disclose the discrimination in azimuth separations for two algorithms, where the initial angles are $(60.25^\circ, 45.39^\circ)$; the azimuth angle incremental interval is $[0.1^\circ, 4.9^\circ]$ with step 0.2°, and the elevation angle incremental interval is $[2^\circ, 50^\circ]$ with step 2°, as shown in Figure 5. We observe that the

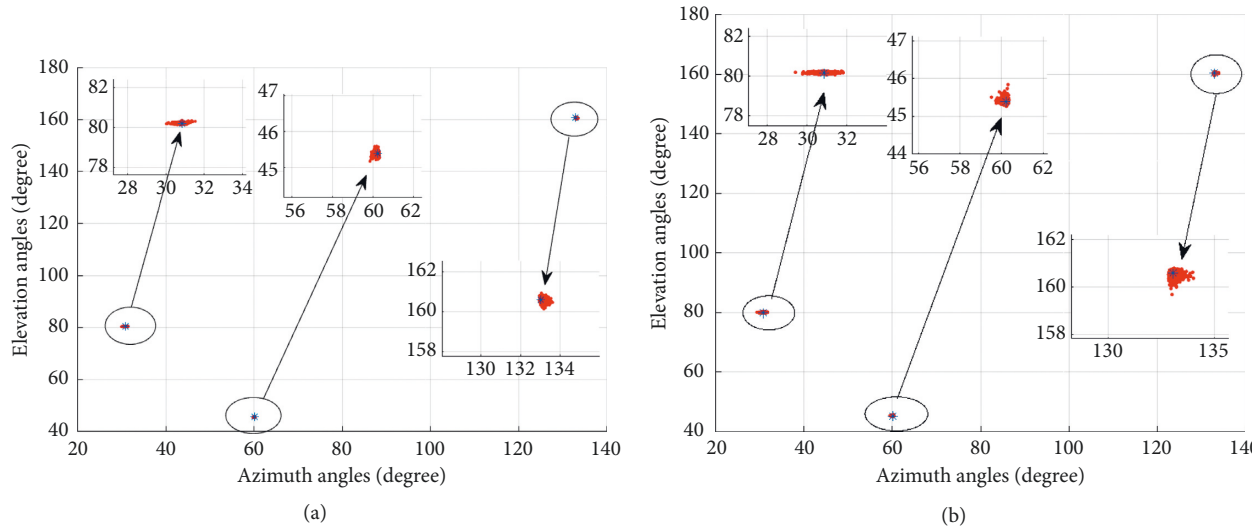

Figure 2: The scatters of 2-D DOA estimation with (a) the subspace-like method and (b) EAET.

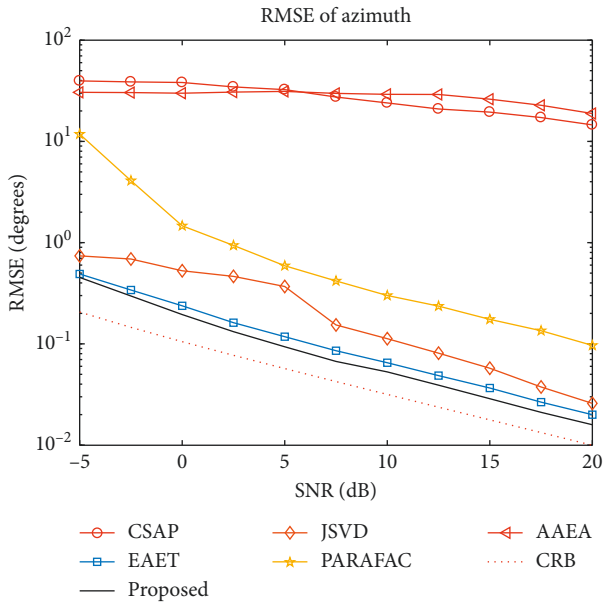

Figure 3: The RMSE of azimuth estimation versus SNR with $K = 3$, $M = 7$, and $J = 500$.

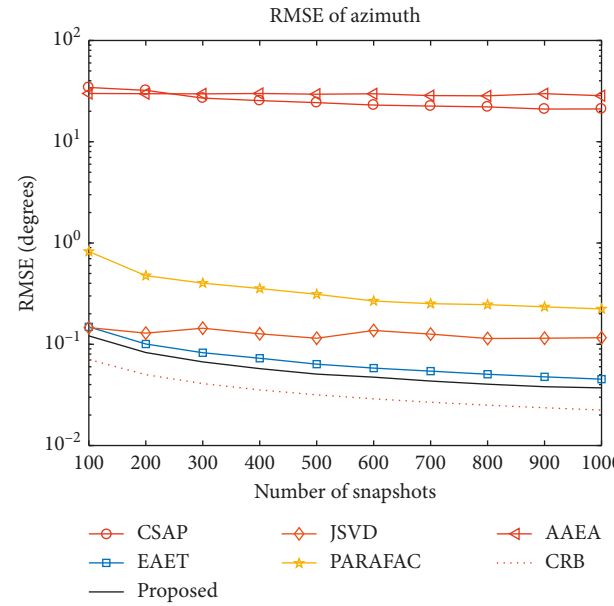

Figure 4: The RMSE of azimuth estimation vs. snapshots with $K = 3$, $M = 7$, and SNR = 10 dB.

proposed subspace-like method has the similar angle discrimination performance as EAET [12].

4.2.5. Complexity vs. Number of Subarray Elements

Example 5. The complexity with respect to the number of subarray elements is presented in Figure 6, where SNR = 10 dB, $J = 500$, $K = 3$, and the range of M is set from 4 to 100 with step 4. We observe that the subspace-like method has relative low running time among the compared methods. It is worth noting that the subspace-like method possesses the best estimation performance when azimuth separation is small, which is particularly suitable for the scenarios where sources are close in spatial azimuths. On the other hand, we observe that the subspace-like method has lower complexity than the PARAFAC method when $M < 100$.

4.2.6. RMSE vs. SNR for the Sparse Reconstruction Methods

Example 6. The performance of the sparse reconstruction methods, with respect to SNR varying from −5 dB to 20 dB with the interval 2.5 dB, is investigated in this example. The angle grids of two basis matrices span $[1°, 180°]$ with step 1°, i.e., $N_\theta = 180$ and $N_\varphi = 180$. Three sources angles are the same as those in Example 2, and other parameters are set the same values as those in Example 1 except SNR. To compare all methods fairly, we take only the azimuth estimation into

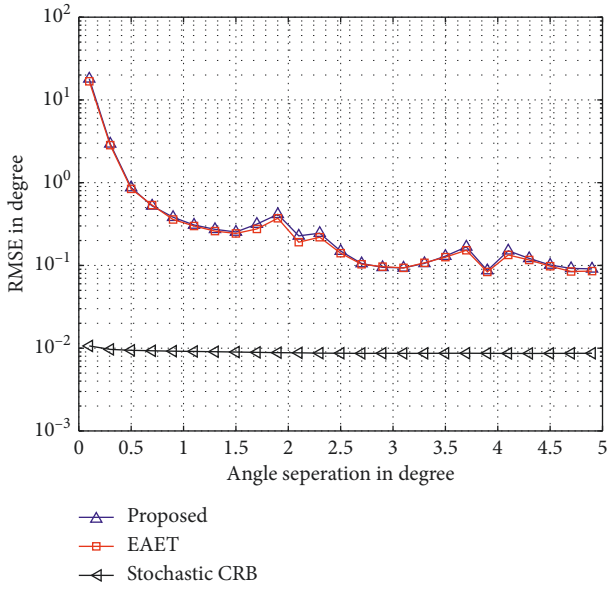

Figure 5: The RMSE of azimuth estimation vs. azimuth separations.

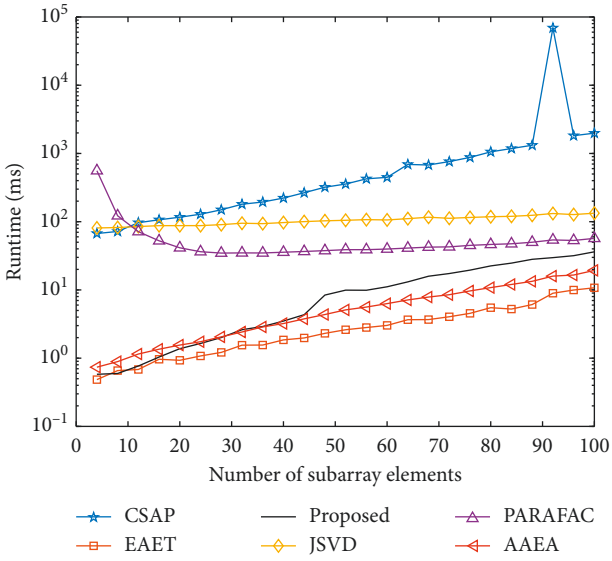

Figure 6: Runtime vs. the number of subarray elements with $K = 3$, $J = 500$, and SNR = 10 dB.

account. The RMSE of azimuth estimation vs. SNR for the sparse reconstruction methods with and without CS involvements are shown in Figure 7. It is observed that the azimuth estimation improves as SNR increases. The (38) performs significantly the best among the methods across the SNR range, which is expected as explained in Section 3.3.2 (see the note), since the sparse reconstruction method using (38) is developed regardless of whether azimuths are apart or close. The performance of (33), as stated in Section 3.3.1 (see the note), is however significantly degraded because azimuth angles are close. On the other hand, the CS versions (41) and (36) perform slightly worse than their counterparts (38) and (33), respectively, and their performance is unstable to

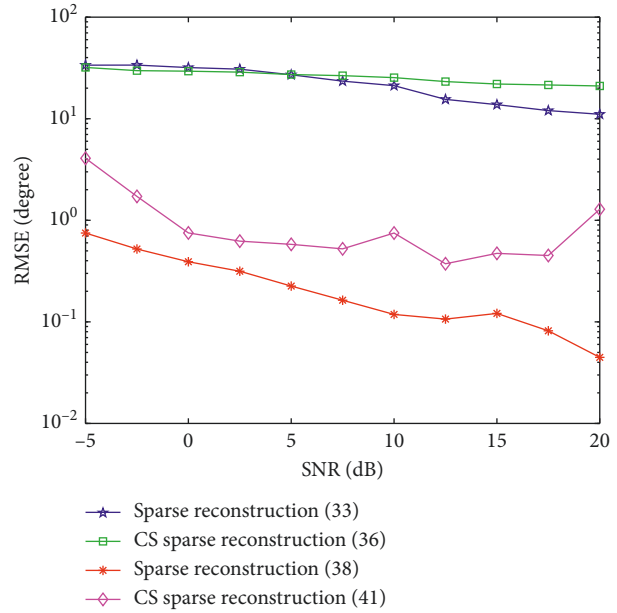

Figure 7: The RMSE of azimuth estimation vs. SNR for sparse reconstruction methods with and without CS involvements.

varying basis matrices during the Monte Carlo trials. Comparing Figure 6 with Figure 3, the RMSE of the sparse reconstruction method using (38) is better than that of JSVD when SNR < 10 dB. Meanwhile, it is superior to PARAFAC.

4.2.7. Complexity vs. Number of Subarray Elements

Example 7. The complexity with respect to the number of subarray elements for the sparse reconstruction methods is presented in Figure 8, where SNR = 10 dB, $J = 500$, $K = 3$, and the range of M is set from 4 to 100 with step 4. We observe that the sparse reconstruction (38) has the lowest running time among the compared methods; it is worth noting that (38) still holds the best azimuth estimation performance. The incorporation of CS into conventional data models leads to higher complexity. By comparing Figures 7 with Figure 5, it is found that the runtime of (38) is less than that of PARAFAC; this can be explained by the fact that the search ranges are set to $[0°, 180°]$ with step 0.1° for PARAFAC, but the same search ranges with step 1° for sparse reconstruction methods, since 0.1° angle separation will destroy coherence of basis matrix and lead to performance degradation. The data models (33), (36), (38), and (41) are computationally comparable with PARAFAC, but more efficient than CSAP [29] and JSVD [18]. The other observation is that there is no significant increase in the complexity for the sparse reconstruction methods with the number of subarray elements, which shows advantages over the competitive methods. Thus, developing applications with large array size is an interesting topic.

4.3. Analysis and Discussion. From all the examples above, it is clearly concluded that the performance benefiting from the generalized virtual received data model can outperform

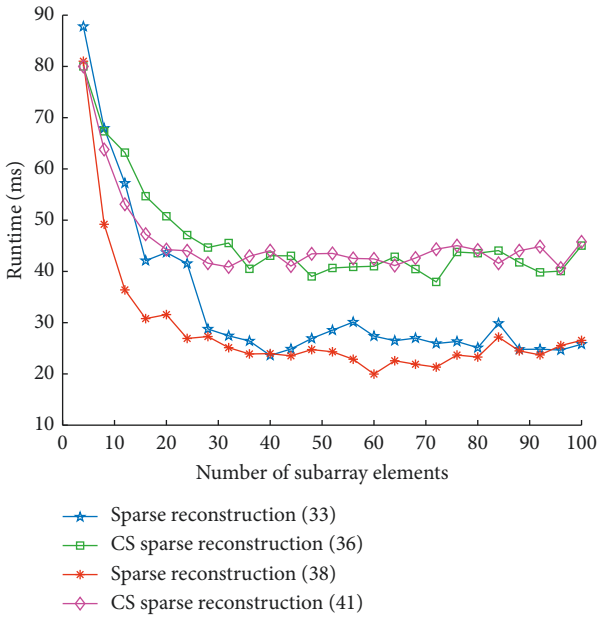

Figure 8: Runtime vs. the number of subarray elements for sparse reconstruction methods with and without CS involvements.

those from the conventional data models. We propose two kinds of methods to address the 2-D DOA estimation. One is the generalization of PM-ESPRIT, referred to as the subspace-like method, which fully utilize generalized virtual aperture to enhance the performance with a low computational complexity. The proposed sparse reconstruction methods provide the general theoretical framework with rigorous proof, which is suitable for any array geometry. Following this, we carry out the derivation of 2-D DOA estimation using partial generalized virtual aperture based on M-FOCUSS and obtain satisfactory results with a moderate computational complexity. One drawback of the proposed methods is that they only deal with the underdetermined signals using doubled elements. This problem to handle overdetermined sources has been addressed in the other paper.

5. Conclusions

In this paper, we exploit both the forward and backward conjugate symmetric properties of the sample cross-correlation matrix of X-subarray and Z-subarray for L-shaped ULA. A generalized virtual received data model is therefore constructed, which improves substantially the azimuth estimation performance. We propose two kinds of approaches to estimate the 2-D DOA with automatic angles pairing. Compared to existing methods, the subspace-like method is efficient when the data model matches the physical model well. On the other hand, the sparse reconstruction methods are able to reduce complexity by converting 2-D search procedures to two successive 1-D search procedures. Numerical examples validate the effectiveness of the theoretical analysis and confirm the superb performance with low complexity for the subspace-like method and with moderate complexity for the sparse reconstruction methods.

Data Availability

The data used to support the findings of this study are available from the corresponding author upon request.

Conflicts of Interest

The authors declare that they have no conflicts of interest.

Acknowledgments

This research was funded by Shandong Province NSF under Grant no. ZR2016FM43, in part by China NSF under Grants nos. 61773059 and 61371169, in part by the National Defense Major Fundamental Research Program of China (Grant no. C×××20110003), the National Defense Key Fundamental Research Program of China (Grant nos. A×××20110005 and A×××20132010), in part by Natural Science Basic Research Project of Shaanxi Province under Grant nos. 2018JQ6046, and China Postdoctoral Science Foundation under Grant 2017M623123.

References

[1] H. L. Van Trees, *Detection, Estimation, and Modulation Theory, Part IV-Optimum Array Processing*, Wiley, Hoboken, NJ, USA, 2004.

[2] Y. Hua, T. K. Sarkar, and D. D. Weiner, "An L-shaped array for estimating 2-D directions of wave arrival," *IEEE Transactions on Antennas and Propagation*, vol. 39, no. 2, pp. 143–146, 1991.

[3] N. Tayem and H. M. Kwon, "L-Shape 2-dimensional arrival angle estimation with propagator method," *IEEE Transactions on Antennas and Propagation*, vol. 53, no. 5, pp. 1622–1630, 2005.

[4] C. P. Mathews and M. D. Zoltowski, "Eigenstructure techniques for 2-D angle estimation with uniform circular arrays," *IEEE Transactions on Signal Processing*, vol. 42, no. 9, pp. 2395–2407, 1994.

[5] P. Strobach, "Two-dimensional equirotational stack subspace fitting with an application to uniform rectangular arrays and ESPRIT," *IEEE Transactions on Signal Processing*, vol. 48, no. 7, pp. 1902–1914, 2000.

[6] J.-F. Gu, W.-P. Zhu, and M. N. S. Swamy, "Joint 2-D DOA estimation via sparse L-shaped array," *IEEE Transactions on Signal Processing*, vol. 63, no. 5, pp. 1171–1182, 2015.

[7] H. Chen, C. Hou, Q. Wang, L. Huang, W. Yan, and L. Pu, "Improved azimuth/elevation angle estimation algorithm for three-parallel uniform linear arrays," *IEEE Antennas and Wireless Propagation Letters*, vol. 14, pp. 329–332, 2015.

[8] W. Rao, D. Li, and J. Zhang, "A tensor-based approach to L-shaped arrays processing with enhanced degrees of freedom," *IEEE Transactions on Signal Processing*, vol. 25, no. 2, pp. 234–238, 2018.

[9] J. A. Zhang, W. Ni, P. Cheng, and Y. Lu, "Angle-of-arrival estimation using different phase shifts across subarrays in localized hybrid arrays," *IEEE Communications Letters*, vol. 20, no. 11, pp. 2205–2208, 2016.

[10] X. Nie and P. Wei, "Array aperture extension algorithm for 2-D DOA estimation with l-shaped array," *Progress in Electromagnetics Research Letters*, vol. 52, pp. 63–69, 2015.

[11] Z. F. Cheng, P. Shui, Y. Zhao, Y. T. Zhu, and H. Li, "Sparse representation based two-dimensional direction-of-arrival

estimation method with L-shaped array," *IET Radar Sonar & Navigation*, vol. 10, no. 5, pp. 976–982, 2016.

[12] Y.-Y. Dong, C.-X. Dong, J. Xu, and G.-Q. Zhao, "Computationally efficient 2-D DOA estimation for L-shaped array with automatic pairing," *IEEE Antennas and Wireless Propagation Letters*, vol. 15, pp. 1669–1672, 2016.

[13] N. Tayem, K. Majeed, and A. A. Hussain, "Two-dimensional DOA estimation using cross-correlation matrix with L-shaped array," *IEEE Antennas and Wireless Propagation Letters*, vol. 15, pp. 1077–1080, 2016.

[14] N. Xi and L. Liping, "A computationally efficient subspace algorithm for 2-D DOA estimation with L-shaped array," *IEEE Signal Processing Letters*, vol. 21, no. 8, pp. 971–974, 2014.

[15] G. Wang, J. Xin, N. Zheng, and A. Sano, "Computationally efficient subspace-based method for two-dimensional direction estimation with L-shaped array," *IEEE Transactions on Signal Processing*, vol. 59, no. 7, pp. 3197–3212, 2011.

[16] J. Liang and D. Liu, "Joint elevation and azimuth direction finding using L-shaped array," *IEEE Transactions on Antennas & Propagation*, vol. 58, no. 6, pp. 2136–2141, 2010.

[17] S. O. Al-Jazzar, D. C. Mclernon, and M. A. Smadi, "SVD-based joint azimuth/elevation estimation with automatic pairing," *Signal Processing*, vol. 90, no. 5, pp. 1669–1675, 2010.

[18] J.-F. Gu and P. Wei, "Joint SVD of two cross-correlation matrices to achieve automatic pairing in 2-D angle estimation problems," *IEEE Antennas and Wireless Propagation Letters*, vol. 6, no. 99, pp. 553–556, 2007.

[19] S. Kikuchi, H. Tsuji, and A. Sano, "Pair-matching method for estimating 2-D angle of arrival with a cross-correlation matrix," *IEEE Antennas and Wireless Propagation Letters*, vol. 5, no. 1, pp. 35–40, 2006.

[20] M. G. Porozantzidou and M. T. Chryssomallis, "Azimuth and elevation angles estimation using 2-D MUSIC algorithm with an L-shape antenna," in *Proceedings of the Antennas and Propagation Society International Symposium*, pp. 1–4, Toronto, Canada, July 2010.

[21] Q. Cheng, Y. Zhao, and J. Yang, "A novel 2-D DOA estimation for coherent signals based on L-shaped array," in *Proceedings of the International Conference on Wireless Communications and Signal Processing*, pp. 1–5, Huangshan, China, October 2013.

[22] R. Cao, C. Wang, and X. Zhang, "Two-dimensional direction of arrival estimation using generalized ESPRIT algorithm with non-uniform L-shaped array," *Wireless Personal Communications*, vol. 84, no. 1, pp. 321–339, 2015.

[23] X. Zhang, L. Xu, L. Xu, and D. Xu, "Direction of departure (DOD) and direction of arrival (DOA) estimation in MIMO radar with reduced-dimension MUSIC," *IEEE Communications Letters*, vol. 14, no. 12, pp. 1161–1163, 2010.

[24] S. Liu, L. Yang, D. Li, and H. Cao, "Subspace extension algorithm for 2D DOA estimation with L-shaped sparse array," *Multidimensional Systems and Signal Processing*, vol. 28, no. 1, pp. 315–327, 2017.

[25] M. Haardt, M. D. Zoltowski, C. P. Mathews, and J. Nossek, "2-D unitary ESPRIT for efficient 2-D parameter estimation," in *Proceedings of the International Conference on Acoustics, Speech, and Signal Processing*, vol. 3, pp. 2096–2099, Detroit, MI, USA, May 1995.

[26] D. Liu and J. Liang, "L-shaped array-based 2-D DOA estimation using parallel factor analysis," in *Proceedings of the 2010 8th World Congress on Intelligent Control and Automation*, pp. 6949–6952, Jinan, China, July 2010.

[27] L. Xu, R. Wu, X. Zhang, and Z. Shi, "Joint two-dimensional DOA and frequency estimation for L-shaped array via compressed sensing PARAFAC method," *IEEE Access*, vol. 6, pp. 1–10, 2018.

[28] S. F. Cotter, B. D. Rao, K. Kjersti Engan, and K. Kreutz-Delgado, "Sparse solutions to linear inverse problems with multiple measurement vectors," *IEEE Transactions on Signal Processing*, vol. 53, no. 7, pp. 2477–2488, 2005.

[29] Y.-Y. Dong, C.-X. Dong, W. Liu, H. Chen, and G.-Q. Zhao, "2-D DOA estimation for L-shaped array with array aperture and snapshots extension techniques," *IEEE Signal Processing Letters*, vol. 24, no. 4, pp. 495–499, 2017.

[30] K. C. Huarng and C. C. Yeh, "A unitary transformation method for angle-of-arrival estimation," *IEEE Transactions on Signal Processing*, vol. 39, no. 4, pp. 975–977, 1991.

[31] K. C. Huarng and C. C. Teh, "Adaptive beamforming with conjugate symmetric weights," *IEEE Transactions on Antennas & Propagation*, vol. 39, no. 7, pp. 926–932, 1991.

[32] Y. Wang and G. Leus, "Space-time compressive sampling array," in *Proceedings of the Sensor Array and Multichannel Signal Processing Workshop*, pp. 33–36, Jerusalem, Israel, October 2010.

[33] I. F. Gorodnitsky and B. D. Rao, "Sparse signal reconstruction from limited data using FOCUSS: a re-weighted minimum norm algorithm," *IEEE Transactions on Signal Processing*, vol. 45, no. 3, pp. 600–616, 1997.